



OPEN ACCESS

Excitonic and vibrational nonlinear processes in a polydiacetylene studied by a few-cycle pulse laser

To cite this article: T Kobayashi *et al* 2008 *New J. Phys.* **10** 065016

View the [article online](#) for updates and enhancements.

You may also like

- [Very high-frequency gravitational waves from magnetars and gamma-ray bursts](#)
Hao Wen, , Fang-Yu Li et al.
- [Energy levels and radiative rates for transitions in Ti X](#)
Kanti M Aggarwal and Francis P Keenan
- [A computational strategy for nonlinear time-fractional generalized Kawahara equation using new eighth-kind Chebyshev operational matrices](#)
H M Ahmed, R M Hafez and W M Abd-Elhameed

Excitonic and vibrational nonlinear processes in a polydiacetylene studied by a few-cycle pulse laser

T Kobayashi^{1,2,3,4,6}, I Iwakura^{1,5} and A Yabushita³

¹ Department of Applied Physics and Chemistry and Institute for Laser Science, University of Electro-Communications, 1-5-1 Chofugaoka, Chofu, Tokyo 182-8585, Japan

² JST, ICORP, Ultrashort Pulse Laser Project, 4-1-8 Honcho, Kawaguchi, Saitama, 332-0012, Japan

³ Department of Electrophysics, National Chiao Tung University, Hsinchu 300, Taiwan

⁴ Institute of Laser Engineering, Osaka University, 2-6 Yamada-oka, Suita, Osaka 565-0971, Japan

⁵ JSPS Research Fellow, 8 Ichibancho, Chiyoda-ku, Tokyo 102-8472, Japan
E-mail: kobayashi@ils.uec.ac.jp

New Journal of Physics **10** (2008) 065016 (15pp)

Received 31 January 2008

Published 30 June 2008

Online at <http://www.njp.org/>

doi:10.1088/1367-2630/10/6/065016

Abstract. High-density excitation of exciton induces the faster decay of absorbance change due to exciton–exciton interaction originated from the Auger recombination process. Experimental results clarified the dynamics of the exciton and the bimolecular quenching rate and the jump rate of exciton were determined to be $5.2 \times 10^{-9} \text{ cm}^3 \text{ s}^{-1}$ and $5.2 \times 10^{-9} \text{ s}^{-1}$, respectively. The intensity modulation of electronic transition under high-density excitation with sub-5-fs pulse was analyzed to observe the Fourier power spectrum of the molecular vibration modes and revealed the existence of a combination tone (2726 cm^{-1}) of the C–C (1241 cm^{-1}) and the C=C (1485 cm^{-1}) stretching modes. This indicates that the highly excited state induced by the Auger process results in the fusion of vibrational quantum states. Difference frequency generation of the vibrational modes also takes place in the same process due to the fission of the vibrational quanta stimulated by the interaction of the two vibrational modes. It was also found that the intensities of several prominent

⁶ Author to whom any correspondence should be addressed.

peaks corresponding to the modes of C=C and C–C stretching were proportional to the squared intensity of the probe pulse. Furthermore, the frequencies of the modes were shifted to low frequencies at high probe intensity. The process can be considered to be fifth-order cascaded Raman scattering via real excitation of vibronic excitons.

Contents

1. Introduction	2
2. Experiment	3
2.1. Material	3
2.2. Laser	4
3. Result and discussion	5
3.1. Pump intensity dependence on the exciton decay dynamics: exciton–exciton interaction	5
3.2. Pump intensity dependence of the molecular vibrational frequency	6
3.3. Probe intensity dependence	10
4. Conclusion	13
Acknowledgments	13
References	13

1. Introduction

Many research groups have studied ultrafast dynamics after photo-excitation of various materials, like molecules in solution [1]–[9] and solid materials [8]–[19]. In the field of basic physics, conjugated polymers are studied as a model reflecting low-dimensional material dynamics. Polydiacetylene (PDA) derivatives form one of the typical groups among various conjugated polymers. PDA has large nonlinearity due to large oscillator strength of exciton, which is a quasi-boson having residual characteristics of fermion introducing the optical nonlinearity. PDA provides interesting subjects to be studied, like its ultrafast relaxation caused by the quasi-one dimensionality and large nonlinearity.

The ultrafast dynamics of PDA after photoexcitation has been explained in terms of the geometrical relaxation (GR) of a free exciton (FE) to a self-trapped exciton (STE) within 100 fs together with the internal conversion (IC) from 1B_u state to 1A_g state [8]–[19]. The STE has been well established to be a geometrically relaxed state with admixture of a butatriene-type chain and an acetylene-type chain [12, 13]. The stretching vibrations of carbon atoms are considered to be coupled to the photogenerated FE and induce various nonlinear optical processes different from those in most inorganic semiconductors [10, 11, 18], [20]–[22]. Recent experimental and theoretical studies have revealed that the lowest excited singlet state in PDA is an optically forbidden 2^1A_g state [19], [23]–[29]. Long conjugation length of PDA substantially stabilizes the energy of the 2^1A_g state to be lower than that of a strongly allowed 1^1B_u –FE state, which provides a characteristic intense blue color and metallic reflection [30]–[35]. The IC from 1^1B_u –FE state to 2^1A_g state mentioned above is then explained to take place along with self-trapping to form STE [20, 21]. However, the detailed dynamical processes of IC and GR have not yet been fully characterized.

Recent progress in femtosecond pulsed lasers has enabled the study of molecular dynamics on a 10 fs timescale [1], [14]–[19]. In the previous works by Bigot and others, a wavepacket motion of C=C stretching mode with a period of ~ 23 fs was found in the photon-echo and transient bleaching signals of PDA–DCAD (poly (1,6-di (*n*-carbazolyl)-2,4 hexadiyne)) films by using 9–10 fs pulses [12, 13]. The real-time observation of GR in PDA has been enabled by the recent development of sub-5-fs visible pulse generation based on non-collinear optical parametric amplification (NOPA) system [36]–[38]. The broadband spectrum of the NOPA enables us to observe the probe wavelength dependence of the real-time signal of the absorbance change ΔA , which is called the ‘real-time spectrum’ of ΔA . By using time-resolved analysis of the Fourier transform of the real-time spectrum, the dynamic features of self-trapping, IC, and coupling between stretching and bending modes in the relaxed state in a PDA have been elucidated using sub-5-fs pulses [19].

In the linear regime, the dynamics of PDA has been studied extensively in our group as mentioned above [8]–[11], [16]–[19]. After getting the information, it is furthermore interesting to study nonlinear dynamics. One of the examples is the nonlinear dynamics due to the bimolecular interaction between two excitations. It is well known that the lifetimes of molecular excited states and Frenkel excitons are reduced under high-density excitation in the crystals of aromatic molecules such as anthracene [39, 40], pyrene [41], and fluoranthene [42], and a charge-transfer complex [43], J aggregates [44] and polymers [45]–[49]. The mechanism of the lifetime shortening is well established to be the Auger process, in which one of the two neighboring excitations (excited molecules or Frenkel excitons) are excited to a higher excitation (higher electronic excited state in a molecule or an excited exciton state) and the other to the ground state by the transition dipole–transition dipole interaction [39]–[42]. Since the Auger quenching takes place when the two excitons are close to each other, the quenching rate (γ) is related to the hopping rate (λ) of excitons as shown and utilized in our previous paper [40]. The higher excitations generated in the Auger process are expected to relax very rapidly to the lowest excited state or the lowest exciton state, resulting in the lifetime shortening of the excitations [42, 43, 47, 48].

The present paper discusses various nonlinear processes observed in PDA. It was found that the intensities of several prominent peaks corresponding to the stretching modes of C=C bond and C–C bond were proportional to the probe pulse intensity. Furthermore, the frequencies of the modes were shifted to low frequencies at high probe intensity. We discovered that highly anharmonic molecular vibration is induced at high-density excitation by the Auger process for the molecular vibrational modes fused to generate the combination tone and difference frequency mode. The latter is a parametric process for the molecular vibrational modes and is the molecular vibrational version of frequency conversion. We could also observe for the first time the vibrational anharmonicity of vibronic excitons in PDA induced by the probe pulse after the pump pulse generates the excitations. This is the cascaded hyper-Raman process through real excitation of vibronic exciton.

2. Experiment

2.1. Material

In this work, a cast film of polydiacetylene-3-butoxycarbonylmethylurethane (PDA-3BCMU) on a glass substrate was used as a sample. The sample absorption and laser spectra are shown in figure 1.

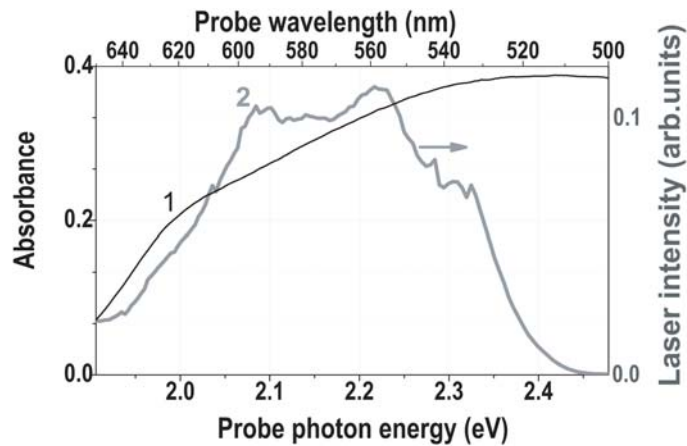


Figure 1. The absorption spectrum of PDA-3BCMU sample film (curve 1) and the spectrum of the 5 fs laser pulse (curve 2).

2.2. Laser

Chirped mirrors were used to obtain shorter pulses than 5 fs [50]–[52]. The second harmonics (150 fs, 100 μ J) of a Ti:sapphire regenerative amplifier (Clark-MXR CPA-1000, 400 μ J, 120 fs, 1 kHz at 790 nm) pumps a 1 mm thick BBO crystal (type-I, 30° z-cut). A single-filament continuum is non-collinearly amplified with the non-collinear internal angle α of 3.7° and the crystal angle θ of 31.5° for the signal-idler group-velocity matching. The tilted-pump geometry with an $\alpha_{\text{apex}} = 45^\circ$ fused-silica (FS) prism with $\phi_1 = 49^\circ$ and a telescope ($f_1 = 200$ and $f_2 = 71$ mm) satisfies the pulse-front-matching (PFM) in the BBO, and the non-tilted signal amplification is attained with elimination of the spatial chirp [52]. Diameters of both beams at the BBO are about 1.5 mm (corresponding to the pump intensity of about 50 GW cm⁻²). Both pump and signal beams are reflected back to the crystal by concave mirrors located in the confocal configuration and the inverse imaging gives the PFM interaction again also in the second-stage amplification with a negligible spectral change. The resulting output pulse energy is 6–7 μ J.

Because the seeded continuum has a chirp, the OPA is a system of chirped-pulse amplification [53]. In order to utilize the full bandwidth, the chirp rate must be small enough for all the spectral components in the bandwidth to interact with the pump pulses in a BBO crystal. A relatively thick sapphire glass plate (2 mm) was used together with a low-frequency cut-off filter before amplification for ultra-stable operation for versatile spectroscopic applications. Pre-compression of the seed [54] is then required for full-bandwidth operation in our setup and after amplification a main compressor compensates the residual part of the chirp. The total pulse compressor is composed of ultra-broadband chirped mirrors (UBCMs, Hamamatsu Photonics), a 45°-FS prism pair, air and 0.5 mm thick Cr-coated broadband beam splitters in a fringe-resolved autocorrelator (FRAC). The UBCMs are specially designed to have appropriate wavelength dependence for the accurate phase compensation over 200 THz in the visible. A UBCM pair with one round trip is used for pre-compression, and another UBCM pair with three round trips and prism pair are for main compression. The parameters of the compressor are determined to cancel the measured group delay (GD) across the whole spectral range. The best compression is attained in the case of a 1 m separation and a 6.0 mm intraprism path length

(IPL) of the prism pair at 650 nm and the net four round trips of the UBCM pairs. The throughput of the compressor is about 80%, which is determined by Fresnel loss at the prism surfaces. The final pulse energy is hence about 5 μ J.

The spectral shape of the signal after the compressor depends on the positions of the delay lines, which are determined to maximize the bandwidth. The full width half maximum (FWHM) is as broad as 240 nm (150 THz) with the corresponding transform-limited (TL) pulse width of 4.4 fs. The expected phase at the entrance of the 10 μ m thick BBO crystal in the FRAC is obtained by frequency integration of the sum of the measured GD of the pulse measured just after amplification and the calculated GD of the compressor. The deviation of the phase is only within $\pm\pi/4$ radian over the whole spectral range.

The pulse shape is measured by the FRAC with low dispersion, where both arms are perfectly balanced by the same beam splitters and the fine delay is on-line calibrated. The sech²-fit pulse width is as short as 3.5 fs. Complex Fourier-transformation (FT) of the spectrum (DIFT) gives the intensity profile with a nearly TL 4.7 fs FWHM, and the calculated FRAC trace agrees very well with the experimental result even in the side wings on both sides. Fitting the trace with parameters of GD dispersion (GDD) and third-order dispersion with inclusion of the oscillating phase of the UBCMs also gives a 4.7 ± 0.1 fs duration [15]. Even though there remains some uncertainty especially in the leading and trailing regions of the intensity profile deduced by this method [55], the FWHM determined by the central part of the pulse is well below 5 fs. A frequency-resolved optical gating (FROG) was measured and found to be consistent with the above result [56]–[59].

3. Result and discussion

3.1. Pump intensity dependence on the exciton decay dynamics: exciton–exciton interaction

Three experiments were performed with the pump pulse intensities of 240, 400 and 840 GW cm⁻², for which corresponding pump photon fluxes were 7.5×10^{29} , 12.5×10^{29} and 26.8×10^{29} photons cm⁻² s⁻¹ with corresponding pump excitation photon densities of 7.5×10^{15} , 12.5×10^{15} and 26.8×10^{15} photons cm⁻², respectively. The intensity of the probe pulses was maintained at 120 GW cm⁻², which corresponds to the photon flux of 3.7×10^{29} photons cm⁻² s⁻¹. Figure 2 shows the difference absorption spectra ΔA averaged over the delay time from 0 to 100 fs. As seen in figure 2, the absorbance change ΔA in the spectral range of the probe pulses extending from 1.9 to 2.0 eV does not depend on the pump intensity, and is almost constant, while that in the spectral range from 2.0 to 2.4 eV increased almost proportionally to the pump intensity.

Figure 3(a) shows the real-time trace of induced absorbance change probed at 16 different probe photon energies at low- and high-density excitations, both of which are highly modulated by the molecular vibration [1, 12, 60]. The density of excited species n is expressed by the following equation:

$$1/n = (\gamma/\alpha + 1/n_0) \exp(\alpha t) - \gamma/\alpha. \quad (1)$$

Here n_0 , α and γ are the initial value of n , the monomolecular and bimolecular decay constants, respectively. In figure 3(b) the inverse of exciton density $1/n$ is plotted against $\exp(\alpha t)$. From the linear relationship between $1/n$ and $\exp(\alpha t)$, α and γ were determined as $6.7 \times 10^{11} \pm 1.0 \times 10^{10}$ s⁻¹ and $5.2 \times 10^{-9} \pm 1.2 \times 10^{-10}$ cm³ s⁻¹, respectively. From the latter, the hopping rate, λ , of the exciton can be determined as $5.2 \times 10^9 \pm 1.2 \times 10^8$ s⁻¹.

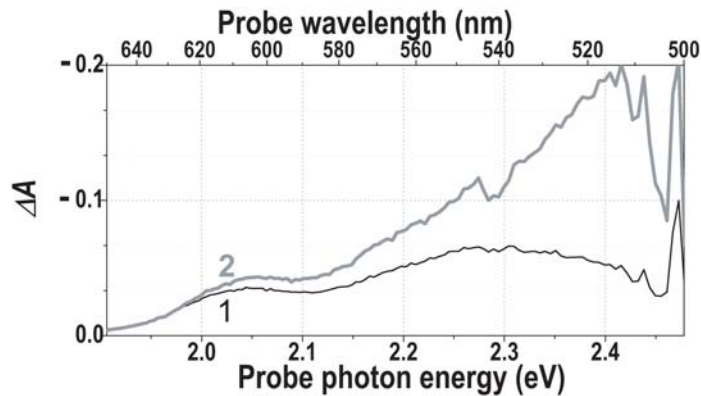


Figure 2. The difference absorbance ΔA averaged over the delay time range from 0 to 100 fs, when the pump intensities were 400 GW cm^{-2} (curve 1) and 840 GW cm^{-2} (curve 2).

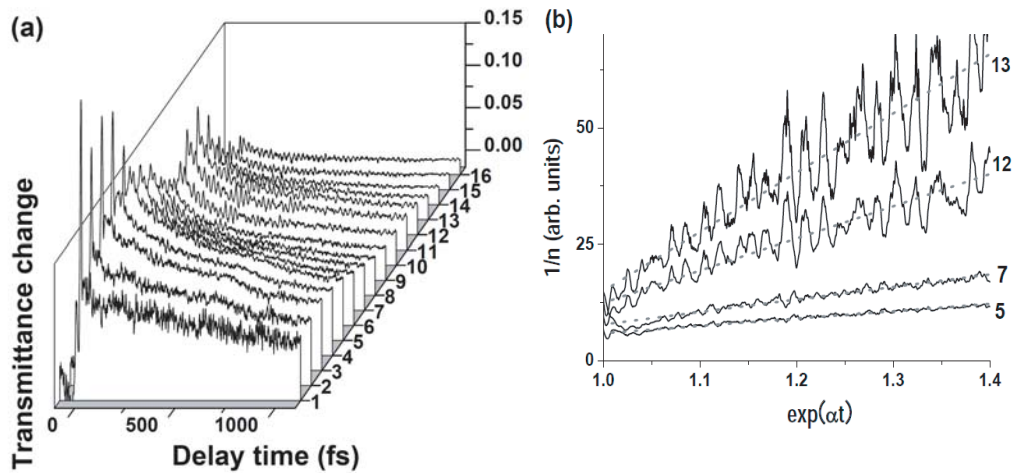


Figure 3. (a) The real-time traces of induced absorbance changes probed at 16 different probe photon energies from -100 fs to 1100 fs, when the pump intensity was 400 GW cm^2 . The wavelengths (probe photon energies) of curves 1 to 16 are as follows: 1, 510 nm (2.479 eV); 2, 510 nm (2.430 eV); 3, 520 nm (2.383 eV); 4, 530 nm (2.338 eV); 5, 540 nm (2.295 eV); 6, 550 nm (2.253 eV); 7, 560 nm (2.213 eV); 8, 570 nm (2.174 eV); 9, 580 nm (2.137 eV); 10, 590 nm (2.100 eV); 11, 600 nm (2.065 eV); 12, 610 nm (2.034 eV); 13, 620 nm (1.999 eV); 14, 630 nm (1.967 eV); 15, 640 nm (1.936 eV) and 16, 650 nm (1.907 eV). (b) The inverse of exciton density $1/n$ is plotted against $\exp(\alpha t)$ for the case of 5, 7, 12 and 13.

3.2. Pump intensity dependence of the molecular vibrational frequency

Figures 4(a) and (b) show the probe wavelength dependence of the Fourier power spectrum of the real-time traces $\Delta A(t)$ in the delay time ranging from 160 to 1100 fs at 16 different wavelengths. The symmetric C–C stretching mode ($\nu_{\text{S-C-C}}$) was observed at 1241 cm^{-1} , which

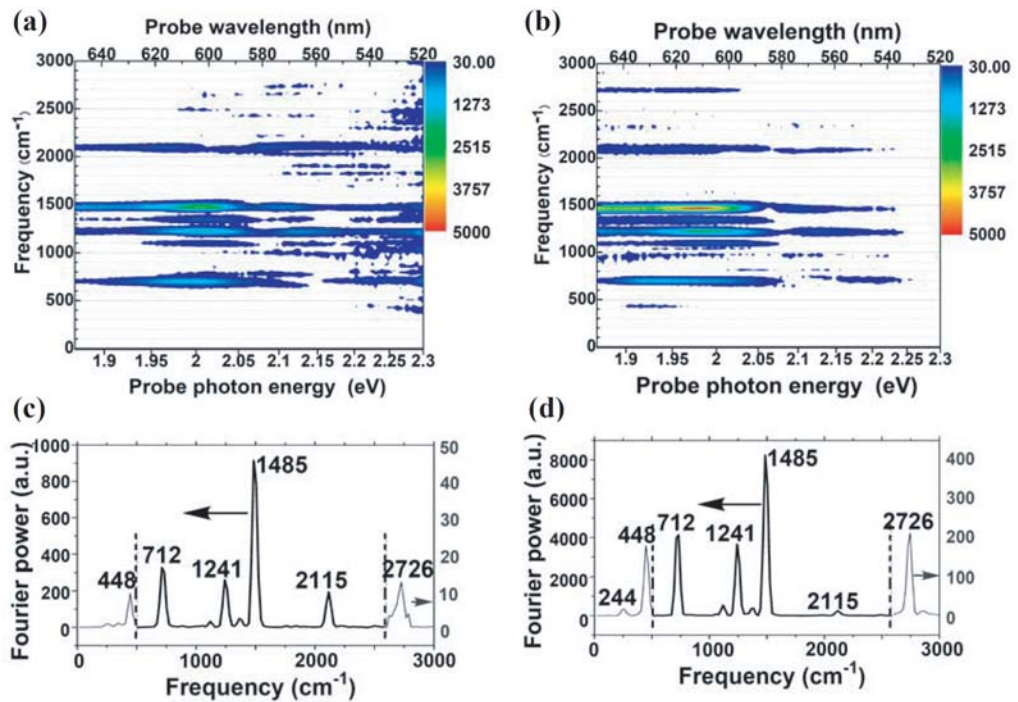


Figure 4. Two-dimensional Fourier power spectra of the ΔA traces in the delay time ranging from 160 to 1100 fs, when the pump intensities were (a) 400 GW cm^{-2} and (b) 840 GW cm^{-2} . Fourier power spectra in the spectral range of probe pulses extending from 1.9 to 2.0 eV, where the induced absorptions were observed, when the pump intensities were (c) 400 GW cm^{-2} and (d) 840 GW cm^{-2} . Thin lines show the Fourier power spectra multiplied by 20 from that of thick line.

is referred to as mode 2. An intense band at 1485 cm^{-1} (mode 3) was assigned to the C=C stretching mode ($\nu_{\text{C}=\text{C}}$). A peak at 2726 cm^{-1} (mode 4), can be assigned to the combination tone between the $\nu_{\text{sC}-\text{C}}$ (1241 cm^{-1}) and the $\nu_{\text{C}=\text{C}}$ (1485 cm^{-1}) [49]. Peaks at 244, 448, 712 and 2116 cm^{-1} were assigned to the modes of C-C=C bending ($\rho_{\text{C}-\text{C}=\text{C}}$), C-C \equiv C-C wagging ($\omega_{\text{C}-\text{C}\equiv\text{C}-\text{C}}$), C-C=C torsion mode ($\tau_{\text{C}-\text{C}=\text{C}}$), and C \equiv C stretching mode ($\nu_{\text{C}\equiv\text{C}}$) [38, 61], respectively. Fourier power spectrum in the spectral range of the induced absorption is shown in figures 4(c) and (d). Relations between the pump intensity and Fourier amplitudes in the spectral range of probe pulses extending from 1.9 to 2.0 eV are shown in figure 5. In these figures, the amplitudes of $\nu_{\text{sC}-\text{C}}$ (mode 2), $\nu_{\text{C}=\text{C}}$ (mode 3), $\omega_{\text{C}-\text{C}\equiv\text{C}-\text{C}}$, and $\tau_{\text{C}-\text{C}=\text{C}}$ with frequencies of 1241, 1485, 448 and 712 cm^{-1} increased nearly proportionally to the pump intensity (see figure 5). On the other hand, the amplitudes of the peaks at 244 and 2726 cm^{-1} were found to be super-linear to the pump intensity. In addition, the peak at 244 cm^{-1} (mode 1) has a frequency which is exactly equal to the difference between 1485 and 1241 cm^{-1} . The previous paper reported that the $\nu_{\text{sC}-\text{C}}$ (1241 cm^{-1}) and the $\nu_{\text{C}=\text{C}}$ (1485 cm^{-1}) were coupled via in-plane bending mode in the main chain (244 cm^{-1}) through Fermi-resonance type interaction [15, 62]. It was found that both $\nu_{\text{sC}-\text{C}}$ (1241 cm^{-1}) and $\nu_{\text{C}=\text{C}}$ (1485 cm^{-1}) modes are modulated in both amplitude and frequency with the modulation frequency of 244 cm^{-1} . This indicates that these three modes

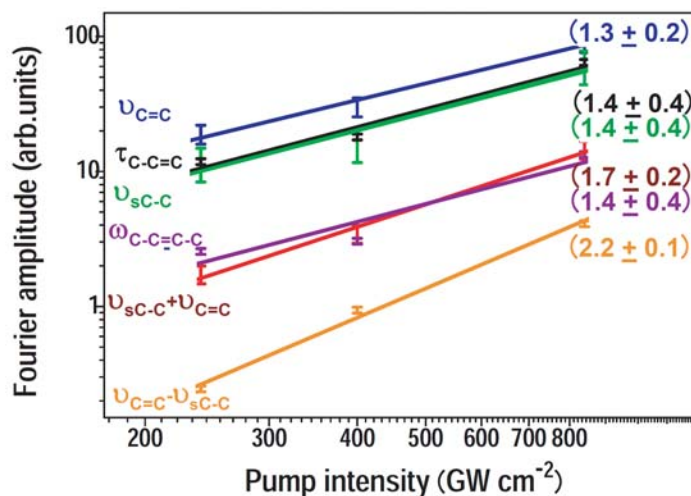


Figure 5. Relation between the pump intensity and Fourier amplitudes in the spectral range of probe pulses extending from 1.9 to 2.0 eV. Six modes correspond to ν_{sC-C} (1241 cm^{-1} : green), $\nu_{C=C}$ (1485 cm^{-1} : blue), $\nu_{C=C} - \nu_{sC-C}$ (244 cm^{-1} : orange), $\nu_{C=C} + \nu_{sC-C}$ (2726 cm^{-1} : red), $\omega_{C-C=C-C}$ (448 cm^{-1} : violet), and $\tau_{C-C=C}$ (712 cm^{-1} : black).

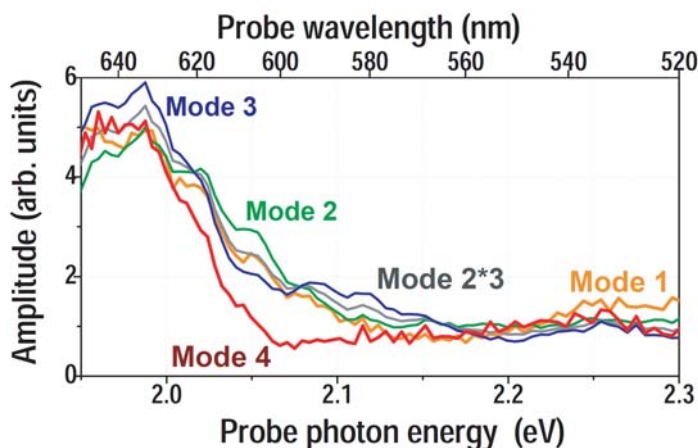


Figure 6. Dependence on the probe photon energy from 1.95 to 2.3 eV of the amplitudes of the five modes with the ν_{sC-C} 1241 cm^{-1} (mode 2: green), the $\nu_{C=C}$ 1485 cm^{-1} (mode 3: blue), the combination tone 244 cm^{-1} (mode 1: orange), 2726 cm^{-1} (mode 4: red) and $1241 * 1485\text{ cm}^{-1}$ (mode 2 * mode 3: gray).

(1485 , 1241 and 244 cm^{-1}) are triangularly coupled with each other. It indicates that the coupling among the relevant three modes is enhanced on high-density excitation.

The decay dynamics was dependent on the pump intensity as discussed before, therefore the Auger process is relevant to the mechanism of the overtone mode (sum frequency) generation process.

Figure 6 shows the probe photon energy dependence of the amplitudes of the modes 1, 2, 3 and 4 and the product of amplitude modes 2 and 3. Amplitudes in the photon energies

between 1.95 and 2.05 eV are relatively higher than those in the other photon energies over all of the modes. The products of the frequencies of the two modes, modes 2 and 3, were found to be in good agreement with those of modes 1 and 4. This also confirms that the combination tone (mode 4) and the difference frequency (mode 1) are both generated by the collision of the vibronic excitations (vibronic exciton) of modes 2 and 3.

In the following, the dynamics of the relevant four modes are to be discussed. Two of them (modes 2 and 3) are the modes directly photo-generated by femtosecond laser and the other two (modes 1 and 4) are generated through the Auger process. Then the dynamics of the envelope of signal amplitudes $c_i(\omega, t)$ of modes i ($i = 1, 2, 3$ and 4) probed at probe photon energy ω can be described as follows:

$$\frac{dc_i(\omega, t)}{dt} = a_i I(\omega, t) - k_i c_i(\omega, t), \quad i = 2, 3, \quad (2)$$

$$\frac{dc_j(\omega, t)}{dt} = b_j c_2(\omega, t) c_3(\omega, t) - k_j c_j(\omega, t), \quad j = 1, 4. \quad (3)$$

The instantaneous amplitude of each mode is given by $c_i(\omega, t)e^{i(\omega_i t + \phi_i)}$ with the frequency of ω_i and the initial phase of ϕ_i . Here $I(\omega, t)$ is the pump laser intensity at probe photon energy ω and local time t . The parameters a_i ($i = 2, 3$) and b_j ($j = 1, 4$) represent the generation efficiency of the relevant modes via direct photo-excitation and the Auger process, respectively. k_i ($i = 1, 2, 3$ and 4) are the decay rates of the vibrational amplitude of the corresponding modes. These equations can be solved as follows.

$$C_i(t) = a_i \int_{-\infty}^t I(t') e^{-k_i(t-t')} dt', \quad i = 2, 3, \quad (4)$$

$$C_j(t) = b_j \int_{-\infty}^t c_2(\omega, t') c_3(\omega, t') e^{-k_j(t-t')} dt' \quad j = 1, 4. \quad (5)$$

The rates k_i were determined as $k_1 = (220 \pm 10 \text{ fs})^{-1}$, $k_2 = (1600 \pm 240 \text{ fs})^{-1}$, $k_3 = (1600 \pm 90 \text{ fs})^{-1}$ and $k_4 = (450 \pm 30 \text{ fs})^{-1}$ from the experimental results of the amplitude dynamics. From (4) and (5), it is expected that the dependence of modes 2 and 3 on the pump pulse intensity are linear while those of modes 1 and 4 are quadratic. Figure 4 shows the pump intensity dependence of the signal intensity, and powers s_i of the intensity dependence I^{s_i} for the four modes were determined to be $s_1 = 2.2 \pm 0.1$, $s_2 = 1.4 \pm 0.4$, $s_3 = 1.3 \pm 0.2$ and $s_4 = 1.7 \pm 0.2$, respectively. These values are consistent with the above expectation. The higher and the lower values of s_1 and s_4 , respectively, than 2 are considered to be due to the effects of higher-order excitation and saturation, respectively. The deviations of the values of s_2 and s_3 to higher values than unity are probably due to the parallel processes of $\omega_2 = \omega_3 - \omega_1$ and $\omega_3 = \omega_4 - \omega_2$ taking place after the creation of ω_3 and ω_4 with small contributions of the modes.

The modulation amplitudes of electronic transitions induced by molecular vibration $c_1(\omega, t)$ and $c_4(\omega, t)$ are expected to be proportional to $c_2(\omega, t)c_3(\omega, t)$, because of the short lifetimes of the corresponding vibrational modes. Since the decay time of the modulation of each mode is independent of probe wavelength, the integrated modulation amplitude $C_k(\omega) = \int_{t_1}^{t_2} c_k(\omega, t) dt$ ($k = 1, 2, 3$ and 4), of these four modes over the probe time range ($t_1 = 0 \text{ fs}$, $t_2 = 1100 \text{ fs}$) are expected to satisfy the relation $C_i(\omega) \propto C_2(\omega)C_3(\omega)$ ($i = 1, 4$). Therefore, the

width of $C_1(\omega)$ (HWHM, $1070 \pm 80 \text{ cm}^{-1}$) and $C_4(\omega)$ (HWHM, $1100 \pm 170 \text{ cm}^{-1}$) are narrower than those of $C_2(\omega)$ (HWHM, $650 \pm 25 \text{ cm}^{-1}$) and $C_3(\omega)$ (HWHM, $2150 \pm 390 \text{ cm}^{-1}$). It agrees with the experimental results that the spectral widths of the modes 1 and 4 are narrower than those of modes 2 and 3 as seen in figure 6.

The above discussion can be rephrased in a slightly different way and the experimental results can be considered to be representing the following reactions between vibrational quanta of different modes taking place. Förster energy-transfer by the transition dipole–transition dipole interaction in the Auger process is associated with the following exchange of vibration quanta,

$$\begin{aligned} (E_1, n_1, n_2, n_3, n_4) + (E_1, n'_1, n'_2, n'_3, n'_4) \\ \rightarrow (E_n, n_1 + 1, n_2, n_3, n_4) + (G, n'_1, n'_2 - 1, n'_3 - 1, n'_4), \end{aligned} \quad (6)$$

$$\begin{aligned} (E_1, n_1, n_2, n_3, n_4) + (E_1, n'_1, n'_2, n'_3, n'_4) \\ \rightarrow (E_n, n_1, n_2, n_3 + 1, n_4 + 1) + (G, n'_1 - 1, n'_2, n'_3, n'_4). \end{aligned} \quad (7)$$

Here, (A, n_1, n_2, n_3, n_4) represents the electronic state A ($= G, E_1$ or E_n) in the ground (G), the lowest excited state (E_1), and higher excited state (E_n) ($n > 1$) coupled with molecular vibrations with n_1, n_2, n_3 and n_4 quanta of modes $\omega_1, \omega_2, \omega_3$ and ω_4 , respectively. The state is a linear combination of such vibronic states with different sets of vibrational quanta (n_1, n_2, n_3 and n_4). Main contributions of n_i ($i = 1, 2, 3$ and 4) are 0 or 1. The equations (6) and (7) are sum and difference frequency generations of molecular vibrations. The latter is a parametric process, which is extensively utilized for frequency conversion and amplification as one of the most important second-order nonlinear optical phenomena.

In the case of collision of two excitons followed by the ‘Auger process’, the electronic energy of an exciton is transferred to the other exciton by the ‘Förster energy transfer’ mechanism resulting in the excitation to the higher excited state with double energy. In this work, we found that the energies of molecular vibrations were also transferred at the same time with the transfer of the electronic energies.

The sum of the molecular vibration frequencies of modes 2 and 3 was nearly equal to the observed molecular vibration frequency of mode 4 referred to the product of modes 2 and 3. It clarifies that the sum of molecular vibration energies is conserved before and after the collisions of vibronic excitons. It was discovered that the molecular vibration and electronic energies are conserved independently even though there are many possible vibrational levels in each of the modes. Thus it was discovered that efficient vibrational energy exchange takes place for modes satisfying sum-frequency or parametric interaction condition from our first direct observation of exchange of vibrational quanta in the Auger process.

3.3. Probe intensity dependence

In this section, the probe intensity dependence of vibrational amplitude keeping the pump intensity constant is studied. The result is shown in figure 7 for the pump intensity of 340 GW cm^{-2} . In this case, the amplitudes of coherent excited molecular vibrations are nearly proportional to the probe light intensity. This result is surprising since the molecular vibration induced by impulsive excitation is expected to be independent of probe intensity.

There are intense peaks at 422, 712, 1241, 2115 and 2726 cm^{-1} . Figure 7 plots the FFT amplitudes calculated for the ΔT signal of these modes against the square of probe intensity.

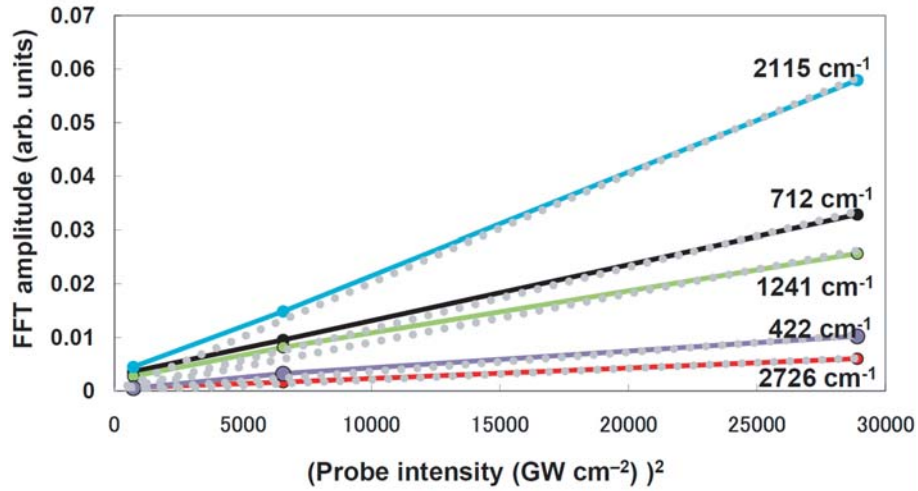


Figure 7. Relation between the square of probe intensity and the Fourier amplitudes calculated for the ΔT signal of 422 (violet), 712 (black), 1241 (green), 2115 (aqua), and 2726 (red) cm^{-1} modes in the spectral range of probe pulses extending from 1.9 to 2.0 eV.

From the figure it is clearly seen that ΔT induced by the Raman active modes have superlinear dependence on the probe intensity. If the relation is described by the following equation:

$$\Delta T = AI^p, \quad (8)$$

the powers of the dependences of the five modes (422, 712, 1241, 2115 and 2726 cm^{-1}) are $p = 2.9, 2.3, 1.8, 2.0$ and 1.7 , in descending mode frequency. The result shows that the signal is proportional to the square power of probe intensity.

In the following, we explain this result by using the semi-classical coupled equations representing the interaction of the electric fields with frequency components of E_L and E_S with frequencies of ω_L and ω_S and coherent molecular vibrational amplitude Q of a representative vibrational mode coupled to the laser field (E_L) and Stokes field (E_S).

In the case of extremely short pulses as used in the present experiment, there are many (continuous) pairs of fields $E_L(\omega_L)$ and $E_S(\omega_S)$, which satisfy the relation of vibrational frequency ω_v to be given by the difference of the two frequencies ω_L and ω_S . If the highest and lowest frequencies of the ultrashort pulse are ω_H and ω_L , respectively, then ω_L and ω_S extend from ω_H and $\omega_L + \omega_v$ and $\omega_H - \omega_v$ and ω_L , respectively, satisfying the above difference relationship.

By utilizing a moving coordinate frame, x', t' with $x' = x$ and $t' = t - x/v$, the stimulated Raman process can be given by the following coupled differential equations:

$$\frac{\partial}{\partial x'} E_S = \kappa_1 E_L Q^*, \quad (9)$$

$$\frac{\partial}{\partial x'} E_L = \kappa_1 E_S Q, \quad (10)$$

$$\left(\frac{\partial}{\partial t'} + \frac{1}{T_2} \right) Q = \kappa_2 E_L E_S^*, \quad (11)$$

$$\left(\frac{\partial}{\partial t'} + \frac{1}{T_2}\right) Q^* = \kappa_2 E_S E_L^*, \quad (12)$$

$$\left(\frac{\partial}{\partial t'} + \frac{1}{T_1}\right) n = \frac{a}{8\hbar} (E_L E_S^* Q^* + E_L^* E_S Q). \quad (13)$$

$$\left(\frac{\partial}{\partial t'} + \frac{1}{T_1}\right) n = \frac{a}{8\hbar} (E_S E_L^* Q + E_S^* E_L Q^*). \quad (14)$$

Here T_2 and T_1 are the vibrational phase (transverse) and population (longitudinal) relaxation times, respectively. κ_1 and κ_2 are the coupling constants. \hbar is the reduced Planck constant and a is a proportionality constant depending on the molecular parameter.

Solutions of (9) and (11) have been obtained in terms of the zeroth and first Bessel functions, I_0 and I_1 , respectively, of complex arguments [64].

$$E_S(x', t') = E_S(0, t') + (bx')^{1/2} E_L(t') \times \int_{-\infty}^{t'} dt'' \exp\left(\frac{t'' - t'}{T_2}\right) \times E_L(t'') E_S(0, t'') [W(t') - W(t'')]^{-1/2} \times I_1(2\{bx'[W(t') - W(t'')]\}^{1/2}). \quad (15)$$

Here, $b = \kappa_1 \kappa_2$ and $W(t) = \int_{-\infty}^t dt' |E_L(t')|^2$, the latter being a measure of the pump energy accumulated up to time t . Introducing solution (15) into (9), one finds

$$Q(x', t') = \kappa_1 \int_{-\infty}^{t'} dt'' \left(\exp \frac{t'' - t'}{T_2}\right) E_L(t'') E_S^*(0, t'') \times I_0(2\{bx'[W(t') - W(t'')]\}^{1/2}). \quad (16)$$

The interaction of the pump pulse and coherent vibration can be described by the above (9)–(12). Here, we neglect the population decay of vibrational levels represented by n in (13) and (16). The initial condition for $Q(t = 0)$ is zero because there is no coherent molecular vibration in the system before laser irradiation.

After the pump pulse is transmitted through the sample, the coherent molecular vibration is left in the material for the time up to the vibrational dephasing time. Then the ultrashort probe pulse with the same spectrum as the pump pulse reaches the sample after a delay time set by the optical delay stage. The interaction between the coherent molecular vibration amplitude Q and short pulse fields E_L and E_S can be given by the same equations (14)–(16). In this case depending on the vibrational phase of coherent molecular vibrations, the field intensities of E_L and E_S are changed by amplification and deamplification and *vice versa*.

In the case of the present work, when the E_L and E_S fields are incident, coherent vibrational amplitude is already finite. This is different from the case of pump pulse, where $Q(t = 0)$ is zero and creation of coherent amplitude is starting from vacuum noise. In the case the probe pulse is amplified, the coherent molecular vibration amplitude is as described above. Furthermore, the trailing edge of the probe pulse is used as a probe of the amplified amplitude. Therefore, the amplitude increases linearly with probe light field as expected from (11) and (12). Then, the vibrational amplitude starts to be proportional to the probe pulse intensity. Because the large amplitude of the molecular vibration can reach anharmonic range on the potential curve, the frequencies observed with a high-density probe pulse become lower than those for the low probe intensity case as can be seen in table 1.

Yan and Mukamel [64] observed picosecond impulsive excitation of acoustic phonon excited by stimulated Brillouin scattering, and found that the amplitude of the acoustic phonon does not increase. Their study clarified that the macroscopic amplitude of the modulation of

Table 1.

Probe intensity (GW cm ⁻²)	55	100	132
$\nu_{C-C\equiv C-C}$ (cm ⁻¹)	423.0	423.0	423.0
$\nu_{C-C=C}$ (cm ⁻¹)	705.6	700.6	700.6
ν_{sC-C} (cm ⁻¹)	1228.3	1218.1	1218.1
$\nu_{C=C}$ (cm ⁻¹)	1475.3	1468.2	1468.2

refractive index change is not because of the change of the microscopic amplitude of molecular vibration but because of the increase of the number of molecules associated with the modulation. However, our present experiment shows that the amplitude of molecular vibration increases as follows. As can be seen in figure 2, the absorption is highly bleached and the absorbance change due to bleaching is saturated when the sample is pumped with high pump energy. This is because collisions of the excitons induce the Auger effect after the pump pulse has created a large number of excitons in the PDA sample, and excited the excitons to higher excited states. Then the probe pulse interacts with excitons via coherent vibronic excitation efficiently, and increases the molecular vibrational amplitudes.

In table 1, the molecular vibrational frequencies of four modes are listed for their different probe intensities, with frequency of 423.0, 705.6, 1228.3 and 1475.3 cm⁻¹ at the weakest probe intensity. All four modes except for the mode of C–C≡C–C bending with the lowest frequency decrease with increasing probe intensity. The process can be considered to be fifth-order cascaded Raman scattering via real excitation of vibronic excitons.

4. Conclusion

In conclusion, we discovered that highly anharmonic molecular vibration is induced on high-density excitation by the Auger process for molecular vibrational modes fused to generate the combination tone and difference frequency mode. The latter is the parametric process for the molecular vibrational modes and is the molecular vibrational version of frequency conversion. We also could observe for the first time the vibrational anharmonicity in vibronic excitons in PDA induced by the probe pulse after the pump pulse generates the excitons. This is the cascaded Raman process through real excitation of vibronic exciton.

Acknowledgments

This work was supported by JSPS to II, the grant MOE ATU Program in NCTU to AY and TK, and the 21st Century COE program on ‘Coherent Optical Science’ to TK.

References

- [1] Wang Q, Schoenlein R W, Peteanu L A, Mathies R A and Shank C V 1994 *Science* **266** 422
- [2] Mathies R A, Cruz C H B, Pollard W T and Shank C V 1988 *Science* **240** 777
- [3] Kobayashi T, Saito T and Ohtani H 2001 *Nature* **414** 531
- [4] Saito T and Kobayashi T 2002 *J. Phys. Chem. A* **106** 9436

- [5] Fujino T, Yamaguchi S and Tahara T 2002 *Bull. Chem. Soc. Japan* **75** 1031
- [6] Bredenbeck J, Helbing J, Sieg A, Schrader T, Zinth W, Renner C, Behrendt R, Moroder L, Wachtveitl J and Hamm P 2003 *Proc. Natl Acad. Sci. USA* **100** 6452
- [7] Schmidtke S J, Underwood D F and Blank D A 2004 *J. Am. Chem. Soc.* **126** 8620
- [8] Yoshizawa M, Hattori Y and Kobayashi T 1993 *Phys. Rev. B* **47** 3882
- [9] Yoshizawa M, Kobayashi T, Fujimoto H and Tanaka J 1982 *J. Phys. Soc. Japan* **56** 338
- [10] Kobayashi T, Yoshizawa M, Stamm U, Taiji M and Hasegawa M 1990 *J. Opt. Soc. Am. B* **7** 1558
- [11] Yoshizawa M, Nishiyama K and Kobayashi T 1993 *Chem. Phys. Lett.* **207** 461
- [12] Bigot J Y, Pham T A and Barisien T 1996 *Chem. Phys. Lett.* **259** 469
- [13] Pham T A, Daunois A, Merle J C, Moigne J L and Bigot J Y 1995 *Phys. Rev. Lett.* **74** 904
- [14] Cerullo G, Lanzani G, Muccini M, Taliani C and De Silvestri S 1999 *Phys. Rev. Lett.* **83** 231
- [15] Vierheilig A, Chen T, Walther P, Kiefer W, Materny A and Zeweil A H 1999 *Chem. Phys. Lett.* **312** 349
- [16] Yoshizawa M, Taiji M and Kobayashi T 1989 *IEEE J. Quantum Electron.* **25** 2532
- [17] Yoshizawa M, Yasuda A and Kobayashi T 1991 *Appl. Phys. B* **53** 296
- [18] Yoshizawa M, Hattori Y and Kobayashi T 1994 *Phys. Rev. B* **49** 13259
- [19] Kobayashi T, Shirakawa A, Matsuzawa H and Nakanishi H 2000 *Chem. Phys. Lett.* **321** 385
- [20] Kobayashi T, Yasuda M, Okada S, Matsuda H and Nakanishi H 1997 *Chem. Phys. Lett.* **267** 472
- [21] Kinugusa J, Shimada S, Matsuda H, Nakanishi H and Kobayashi T 1998 *Chem. Phys. Lett.* **287** 639
- [22] Yoshizawa M, Kubo A and Saikan S 1999 *Phys. Rev. B* **60** 15632
- [23] Lawrence B, Torruellas W E, Cha M, Sundheimer M L, Stegeman G I, Meth J, Etemad S and Baker G 1999 *Phys. Rev. Lett.* **73** 1994
- [24] Lavrentiev M Y and Barford W 1999 *Phys. Rev. B* **59** 15048
- [25] Tavan P and Schulten K 1987 *Phys. Rev. B* **36** 4337
- [26] Hayden W and Mele E J 1986 *Phys. Rev. B* **34** 5484
- [27] Hudson B S, Kohler B E and Schulten K 1982 *Excited States* vol 6 (New York: Academic)
- [28] Lanzani G, Cerullo G, Zavelani-Rossi M, De Silvestri S, Comoretto D, Musso G and Dellepiane G 2001 *Phys. Rev. Lett.* **87** 187402
- [29] Gradinaru C C, Kennis J T M, Papagiannakis E, van Stokkum I H M, Cogdell R J, Fleming G R, Niederman R A and van Gronde R 2001 *Proc. Natl Acad. Sci. USA* **98** 2364
- [30] Heeger A J, Kivelson S, Schrieffer J R and Su W P 1988 *Rev. Mod. Phys.* **60** 781
- [31] Su W P, Schrieffer J R and Heeger A J 1980 *Phys. Rev. B* **22** 2099
- [32] Su W P, Schrieffer J R and Heeger A J 1982 *Phys. Rev. Lett.* **68** 1148
- [33] Abe S, Yu J and Su W P 1992 *Phys. Rev. B* **45** 8264
- [34] Abe S, Schreiber M, Su W P and Yu J 1992 *Phys. Rev. B* **45** 9432
- [35] Pakbaz K, Lee C H, Heeger A J, Hagler T W and McBranch D 1994 *Synth. Met.* **64** 295
- [36] Shirakawa A and Kobayashi T 1998 *Appl. Phys. Lett.* **72** 1476
- [37] Cerullo G, Nisoli M, Stagira S, De Silvestri S, Tempea G, Krausz F and Ferencz K 2000 *Appl. Phys. B* **70** S253
- [38] Baltuška A and Kobayashi T 2002 *Appl. Phys. B* **75** 427
- [39] Bergman A, Levine M and Jortner J 1967 *Phys. Rev. Lett.* **18** 593
- [40] Kobayashi T and Nagakura S 1974 *Mol. Cryst. Liq. Cryst.* **26** 33
- [41] Inoue A, Yoshihara K and Nagakura S 1972 *Bull. Chem. Soc. Japan* **45** 1973
- [42] Kobayashi T and Nagakura S 1972 *Mol. Phys.* **24** 695
- [43] Ho Z Z and Peyghambarian N 1988 *Chem. Phys. Lett.* **148** 107
- [44] Minoshima K, Taiji M, Misawa K and Kobayashi T 1994 *Chem. Phys. Lett.* **218** 67
- [45] Adachi S, Kobryanskii V M and Kobayashi T 2002 *Phys. Rev. Lett.* **89** 027401
- [46] Terasaki A, Hosoda M, Wada T, Tada H, Koma A, Yamada A, Sasabe H, Garito A F and Kobayashi T 1992 *J. Phys. Chem.* **96** 10534
- [47] Williams V S, Mazumdar S, Armstrong N R, Ho Z Z and Peyghambarian N 1992 *J. Phys. Chem.* **96** 4500

- [48] Kobayashi T, Fuji T, Ishii N and Goto H 2001 *J. Lumin.* **94–95** 667
- [49] Gulbinas V, Chachisvilis M, Valkunas L and Sundstrom V 1996 *J. Phys. Chem.* **100** 2213
- [50] Shirakawa A, Sakane I and Kobayashi T 1998 *Ultrafast Phenomena XI* ed T Elsaesser *et al* (Berlin: Springer) p 54
- [51] Shirakawa A, Sakane I, Takasaka M and Kobayashi T 1999 *Appl. Phys. Lett.* **74** 2268
- [52] Shirakawa A, Sakane I and Kobayashi T 1998 *Opt. Lett.* **23** 1292
- [53] Dubietis A, Jonusauskas G and Piskarskas A 1992 *Opt. Commun.* **88** 437
- [54] Gale G M, Hache F and Cavallari M 1998 *IEEE J. Sel. Top. Quantum Electron.* **4** 224
- [55] Baltuska A, Wei Z, Pshenichnikov M S, Wiersma D A and Szipöcs R 1997 *Appl. Phys. B* **65** 175
- [56] Baltuska A, Pshenichnikov M S and Wiersma D A 1998 *Opt. Lett.* **23** 1474
- [57] Baltuska A and Kobayashi T 2002 *Appl. Phys. B* **75** 427
- [58] Baltuska A, Fuji T and Kobayashi T 2002 *Phys. Rev. Lett.* **88** 133901
- [59] Baltuska A, Fuji T and Kobayashi T 2002 *Opt. Lett.* **27** 306
- [60] Ikuta M, Yuasa Y, Kimura T, Matsuda H and Kobayashi T 2004 *Phys. Rev. B* **70** 214301
- [61] Kobayashi T, Shirakawa A, Matsuzawa H and Nakanishi H 2000 *Chem. Phys. Lett.* **321** 385
- [62] Vierheilig A, Chen T, Waltner P, Kiefer W, Materny A and Zewail A H 1999 *Chem. Phys. Lett.* **312** 349
- [63] Carman R L, Shimizu F, Wang C S and Bloembergen N 1970 *Phys. Rev. A* **2** 60
- [64] Yan Y J and Mukamel S 1991 *J. Chem. Phys.* **94** 997